

Regression and Classification with Single-Qubit Quantum Neural Networks

Leandro C. Souza^{a,b}, Bruno C. Guingo^{a,c,d}, Gilson Giraldi^a, Renato Portugal^{a,c}

^a*LNCC, Av. Getulio Vargas, 333, Petrópolis, 25651-075, RJ, Brazil*

^b*UFPB, Rua dos Escoteiros, s/n, João Pessoa, 58051-900, PB, Brazil*

^c*UCP, Rua Barão do Amazonas, 124, Petrópolis, 25685-100, RJ, Brazil*

^d*FAETERJ, Av. Getulio Vargas, 335, Petrópolis, 25651-070, RJ, Brazil*

Abstract

Since classical machine learning has become a powerful tool for developing data-driven algorithms, quantum machine learning is expected to similarly impact the development of quantum algorithms. The literature reflects a mutually beneficial relationship between machine learning and quantum computing, where progress in one field frequently drives improvements in the other. Motivated by the fertile connection between machine learning and quantum computing enabled by parameterized quantum circuits, we use a resource-efficient and scalable Single-Qubit Quantum Neural Network (SQQNN) for both regression and classification tasks. The SQQNN leverages parameterized single-qubit unitary operators and quantum measurements to achieve efficient learning. To train the model, we use gradient descent for regression tasks. For classification, we introduce a novel training method inspired by the Taylor series, which can efficiently find a global minimum in a single step. This approach significantly accelerates training compared to iterative methods. Evaluated across various applications, the SQQNN exhibits virtually error-free and strong performance in regression and classification tasks, including the MNIST dataset. These results demonstrate the versatility, scalability, and suitability of the SQQNN for deployment on near-term quantum devices.

Keywords: quantum machine learning, quantum neuron, quantum neural network, parameterized quantum circuit, quantum regression and classification

1. Introduction

Classical machine learning, particularly through artificial neural networks, has transformed many fields by enabling pattern recognition, prediction, and complex decision-making tasks. The neuron, a computational unit inspired by biological neurons [1], is at the core of these networks. One of the earliest models, the perceptron [2], functions as a binary classifier, producing an output based on a weighted sum of inputs [3]. This foundational unit, though limited in complexity, enables the construction of multilayered architectures that drive advancements in support vector machines and deep learning [4].

Quantum computing has opened new frontiers in machine learning, leading to the development of quantum machine learning models that exploit quantum mechanics to achieve computational advantages over classical approaches [5, 6, 7, 8]. However, some authors dispute this assertion [9]. Among these models, Quantum Neural Networks (QNNs) have attracted particular interest because they use quantum parallelism and entanglement to process high-dimensional data more efficiently than classical neural networks. Some of these architectures employ quantum

analogues of classical neurons (quantum neurons or quantum perceptrons) [10, 11, 12, 13]. Unlike classical perceptrons, which operate through deterministic functions, quantum neurons can employ probabilistic mechanisms intrinsic to quantum measurements, allowing them to simulate more general non-linear activation functions [14].

Recent work in QNNs has expanded beyond basic architectures to explore specialized quantum algorithms that could drive new paradigms in neural network design [15, 16, 17, 18, 19, 20, 21]. Early QNN models provided a foundation for applying quantum principles to neural networks by developing frameworks for supervised and unsupervised learning, introducing novel approaches that take advantage of quantum superposition and entanglement [22, 23]. These advances have inspired diverse architectures, such as quantum versions of classical neural network models, and have prompted further research into implementing quantum neurons as functional analogues of classical units in quantum hardware [24]. The introduction of quantum-specific methods, including quantum phase estimation and amplitude amplification, has enabled the creation of probabilistic threshold mechanisms, positioning quantum perceptrons as essential components in advanced QNN designs. Collectively, these developments highlight the potential of QNNs to handle complex data structures and drive innovation in areas where classical neural networks encounter scalability limits [25, 26].

Parameterized quantum circuits (PQCs) play a central role in quantum machine learning, where they serve as flexible and tunable quantum models for learning tasks [27, 28]. A PQC consists of a sequence of quantum gates whose rotation angles, or other parameters, are adjusted during training to optimize the circuit output for a specific objective, such as regression or classification [29]. These circuits can exploit the unique properties of quantum mechanics to represent complex, high-dimensional data in ways that may be challenging for classical models. In quantum machine learning applications, PQCs are often embedded within hybrid quantum-classical algorithms, where classical optimization techniques, such as gradient descent, are used to iteratively update the parameters. This iterative tuning process enables PQCs to learn complex patterns in data, making them adaptable to various tasks and a promising framework to develop quantum neural networks that could outperform their classical counterparts [30].

In addition to their adaptability, PQCs offer a practical means to reduce the complexity of QNNs. By enabling quantum models to achieve higher expressivity with fewer qubits, PQCs can streamline QNN architectures, making them more feasible for current NISQ quantum hardware [27, 31]. This reduction in qubit requirements allows for more efficient circuit designs that maintain robust learning capabilities. The ultimate simplification in this approach is a QNN composed of streamlined single-qubit neurons, where expressivity is maximized through a carefully chosen set of parameterized rotations. In this paper, we focus on this minimal architecture, proposing a QNN model built from single-qubit neurons with tunable angles. This model leverages the power of PQCs to represent complex patterns with minimal resources.

There is growing interest in employing single-qubit quantum processors for machine learning applications [32, 33, 34, 35, 36, 37, 38, 39, 40]. Refs. [32, 33] leverage the 1-qubit deterministic quantum computing model [41] to efficiently estimate classically intractable kernel functions for machine learning tasks, highlighting the role of quantum discord and quantum coherence in achieving computational advantages. Ref. [34] uses single-qubit rotation operators combined with data re-uploading and classical subroutines to construct a quantum classifier capable of handling primarily three-dimensional or lower-dimensional inputs and producing three-category or fewer outputs. This work emphasizes the importance of data re-uploading and single-qubit processing units in overcoming the apparent limitations of single-qubit systems, validating their ability to

classify complex data through extensive benchmarking. Ref. [35] demonstrates that a single-qubit quantum circuit, leveraging the re-uploading of independent variables and optimized parameters, can effectively approximate any bounded complex function. It provides both theoretical proofs and experimental validation on a superconducting qubit device, highlighting the potential of this approach in quantum machine learning applications. Refs. [36, 37, 38, 40] build upon the model developed in Ref. [34] to further explore the potential of single-qubit systems in addressing a wide range of classical machine learning tasks, including supervised, unsupervised, and reinforcement learning. These studies demonstrate comparable or improved performance over classical methods while enabling efficient implementations on low-resource hardware.

In this work, we use a parameterized QNN architecture built on neurons modeled with a single qubit, that generalizes the proposal of Ref. [34] by using a different data re-uploading strategy that can easily handle multi-dimensional inputs, while Ref. [34] accommodates multi-dimensional inputs by dividing them into multiple three-dimensional inputs, increasing the number of layers. The Single-Qubit Quantum Neural Network (SQQNN) provides a framework for efficient machine learning applications through a streamlined sequence of parameterized single-qubit neurons. Using single-qubit neurons, the SQQNN achieves a powerful and versatile architecture capable of addressing both regression and binary classification tasks. This design offers significant advantages, including reduced hardware requirements, simpler implementation, and faster execution on current quantum processors. Furthermore, single-qubit neurons enable the efficient representation of probabilistic activation functions through parameterized quantum measurements, making the SQQNN particularly resource-efficient and well-suited for near-term quantum hardware. This approach offers a practical alternative to multi-qubit models, suitable for early-stage quantum devices.

The theoretical foundation of the SQQNN is built on the most general single-qubit unitary operator, with parameterized input states and measurement observables that adapt based on input data and weights. We validate the model’s capabilities through various applications, demonstrating its effectiveness in both regression and classification tasks. The SQQNN is successfully trained to evaluate a wide range of logical gates, achieving near-zero error and handling both linear and non-linear relationships with ease. It also performs well in more complex binary classification problems, where increasing the number of layers can lead to substantial error reduction. The number of layers indicates the degree of non-linearity with respect to the data input. These results highlight the adaptability and scalability of SQQNN, showcasing its potential as a practical and efficient quantum neural network for diverse machine learning applications.

To train the SQQNN, we employed two distinct learning methods: gradient descent and an improved matrix inversion method. The improved method leverages a matrix constructed from the dataset inputs and powers of their entries, inspired by a truncated Taylor series. This approach helps to find the approximation of complex relationships within the data. Gradient descent was applied to tasks such as logic gate evaluation and datasets regression, while the improved global optimization method proved effective for classification tasks. The network was evaluated on both synthetic and real-world datasets, consistently showing strong performance. The SQQNN achieved promising results on the MNIST dataset with low times, showcasing its scalability and ability to handle high-dimensional, real-world problems. These results emphasize the efficacy of the training methods and the versatility of the SQQNN across diverse machine-learning applications.

The structure of this paper is as follows: In Sec. 2, we define our proposal for the quantum neuron, which is based on a single qubit and designed for supervised learning tasks. In Sec. 3,

we extend this model to the Single-Qubit Quantum Neural Network (SQQNN), detailing its architecture and emphasizing its flexibility and applicability to both regression and classification tasks. In Sec. 4, we describe the training methods used, including gradient descent and the polynomial-based Linear Least Squares, tailored to optimize the SQQNN’s performance. In Sec. 5, we evaluate the SQQNN’s effectiveness in regression tasks. We present experiments that showcase the SQQNN’s ability to accurately model logical gates such as AND, OR, and XOR, as well as its performance on both synthetic functions, like the sinc function, and real-world datasets, including the Combined Cycle Power Plant and Communities Crime datasets. In Sec. 6, we assess the classification performance of the SQQNN on diverse datasets, including synthetic data (Two Moons) and real-world challenges like the Wisconsin Breast Cancer Dataset and MNIST. Finally, in Sec. 7, we summarize our findings and discuss the potential implications and future directions of this work.

2. Single-Qubit Neuron Model

A quantum neuron is a quantum-inspired adaptation of the classical neuron, designed for supervised learning tasks. Given a dataset

$$\mathbb{D} = \{(x_1, y_1), (x_2, y_2), \dots, (x_n, y_n)\} \subset \mathbb{R}^p \times [-1, 1], \quad (1)$$

where each input $x_i \in \mathbb{R}^p$ is a feature vector and each corresponding output $y_i \in [-1, 1]$ is the goal of the quantum neuron. Quantum computational principles are applied to predict the output y for an untested input $x \in \mathbb{R}^p$. The weights of the quantum neuron are encoded within the angles of 1-qubit rotation gates

$$R_x(\theta) = \begin{bmatrix} \cos \frac{\theta}{2} & -i \sin \frac{\theta}{2} \\ -i \sin \frac{\theta}{2} & \cos \frac{\theta}{2} \end{bmatrix}, \quad R_y(\theta) = \begin{bmatrix} \cos \frac{\theta}{2} & -\sin \frac{\theta}{2} \\ \sin \frac{\theta}{2} & \cos \frac{\theta}{2} \end{bmatrix}, \quad R_z(\theta) = \begin{bmatrix} e^{-i\theta/2} & 0 \\ 0 & e^{i\theta/2} \end{bmatrix}.$$

Those gates are combined to build a general unitary operator that depends on three real parameters. Since the most general 1-qubit unitary operator can be expressed as $e^{i\alpha} R_z(\beta) R_y(\gamma) R_z(\gamma)$ [42], we employ the most general single-qubit quantum neuron \mathcal{N} , modulo a global phase, as

$$\mathcal{N} = R_z(\gamma) R_y(\beta) R_z(\alpha). \quad (2)$$

Fig. 1 depicts the most general version the single-qubit quantum neuron together with its input and a measurement. The output depends on the angles $\alpha(x)$, $\beta(x)$, and $\gamma(x)$, which are functions of the data input with a weight vector and are used in the rotation gates R_y and R_z . The input to the circuit is the quantum state $|\psi\rangle = \cos(\theta/2)|0\rangle + e^{i\phi} \sin(\theta/2)|1\rangle$, where θ and ϕ are two extra parameters.

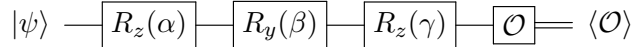


Figure 1: Representation of the most general quantum neuron with an arbitrary input and measurement. The output corresponds to the average value obtained from measuring the observable \mathcal{O} .

After applying the rotation gates, an observable \mathcal{O} is measured. The observable can be decomposed in terms of orthogonal projections as $\mathcal{O} = \lambda_0 \mathcal{P}_0 + \lambda_1 \mathcal{P}_1$, where λ_0 and λ_1 are real

numbers, projection \mathcal{P}_1 is defined as

$$\mathcal{P}_1 = \begin{bmatrix} \cos^2 \frac{\omega}{2} & e^{-i\varphi} \cos \frac{\omega}{2} \sin \frac{\omega}{2} \\ e^{i\varphi} \cos \frac{\omega}{2} \sin \frac{\omega}{2} & \sin^2 \frac{\omega}{2} \end{bmatrix}, \quad (3)$$

and its orthogonal complement is $\mathcal{P}_0 = I - \mathcal{P}_1$, so that the measurement outcome is either λ_0 or λ_1 . Without loss of generality, we set $\lambda_0 = +1$ and $\lambda_1 = -1$. Note that the output of the quantum neuron is not the measurement outcome but the average $\langle \mathcal{O} \rangle$. Since quantum computers usually has only measurement in the computational basis, to implement the measurement of \mathcal{O} , we replace \mathcal{O} with the unitary operator

$$U_{\mathcal{O}} = \begin{bmatrix} \cos \frac{\omega}{2} & -e^{-i\varphi} \sin \frac{\omega}{2} \\ e^{i\varphi} \sin \frac{\omega}{2} & \cos \frac{\omega}{2} \end{bmatrix},$$

obtained from the 1-eigenvectors of \mathcal{P}_0 and \mathcal{P}_1 , followed by a measurement in the computational basis.

The output of the quantum neuron is defined as

$$y = \langle \mathcal{O} \rangle = 1 - 2 |\langle 1 | U_{\mathcal{O}} R_z(\gamma) R_y(\beta) R_z(\alpha) | \psi \rangle|^2,$$

which represents the average of the observable \mathcal{O} . The basis change generated by $U_{\mathcal{O}}$ converts results obtained by measuring Pauli Z into an arbitrary observable \mathcal{O} .

Using the definition of the rotation gates, we obtain

$$y = \cos \beta \cos \theta \cos \omega - \sin \beta \sin \theta \cos \omega \cos(\alpha + \phi) - \sin \beta \cos \theta \sin \omega \cos(\gamma - \varphi) + \sin \theta \sin \omega \sin(\alpha + \phi) \sin(\gamma - \varphi) - \cos \beta \sin \theta \sin \omega \cos(\alpha + \phi) \cos(\gamma - \varphi), \quad (4)$$

where the angles are considered functions of x with parameters representing weights. With this expression, we can not only obtain good estimates for α , β , and γ through the learning process, but also fine-tune the input state and the observable based on the dataset.

All parameters of the circuit of Fig. 1 are present in the expression of the average $\langle \mathcal{O} \rangle$, represented by y in Eq. (4), including the parameters θ , ϕ , ω , and φ that define the input state $|\psi\rangle$ and the basis rotation. We can set $\phi = \varphi = 0$, without loss of generality, indicating that phases are unnecessary in both the initial state and the projection operators.

Taking $\omega = 0$ in Eq. (4), which corresponds to a measurement in the computational basis, we obtain

$$y = \cos \beta \cos \theta - \cos \alpha \sin \beta \sin \theta. \quad (5)$$

In this case, the observable is fixed and cannot be trained. This expression is the most general if we decide to measure in the computational basis. If we further simplify and use $|0\rangle$ as the input to the circuit by setting $\theta = 0$, the outcome of the neuron, which is the average probability after a measurement in the computational basis is

$$y = 1 - 2 |\langle 1 | R_y(\beta) | 0 \rangle|^2 = \cos \beta. \quad (6)$$

This indicates that, in this case, only the R_y gate, parameterized by a single trainable angle β , is required. Fig. 2 shows the reduced version of the quantum neuron, measured in the computational basis.

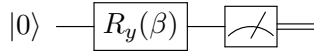


Figure 2: Illustration of the reduced quantum neuron with a fixed input state and measurement in the computational basis.

When measured in the computational basis ($\omega = 0$), y simplifies and no longer depends on γ , as seen in Eq. (5). Furthermore, if the input state is also fixed ($\theta = 0$), the outcome depends solely on a single real parameter, β , as shown in Eq. (6). We apply this reduced neuron model to various examples, such as MNIST classification, demonstrating its effectiveness in these cases.

In the next section, we describe a single-qubit quantum neural network that is composed of neurons as depicted in Fig. 1 and a reduced version that is composed of neurons as depicted in Fig. 2.

3. Single-Qubit Quantum Neural Network

We describe a Single-Qubit Quantum Neural Network (SQQNN) model that uses the interconnection of single-qubit neurons in a streamlined manner. Consider a multi-neuron QNN composed of K neurons ($\mathcal{N}_1, \mathcal{N}_2, \dots, \mathcal{N}_K$), each embodying a single-qubit architecture as depicted in Fig. 3. In this configuration, each neuron \mathcal{N}_k is defined by the sequence $\mathcal{N}_k = R_z(\gamma_k)R_y(\beta_k)R_z(\alpha_k)$, for $k = 1, \dots, K$, where α_k, β_k , and γ_k are trainable parameters specific to each neuron. The input state $|\psi\rangle$ and the observable \mathcal{O} each have a single trainable parameter that is not associated with individual neurons. The SQQNN is applicable to both regression and classification tasks.

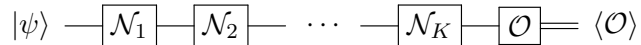


Figure 3: Representation of the SQQNN with an arbitrary input and measurement. The output is the average value obtained from measuring the observable \mathcal{O} . Each neuron \mathcal{N}_k has three trainable parameters, while the input state $|\psi\rangle$ and the observable \mathcal{O} each have a single trainable parameter, since we have set $\phi = \varphi = 0$.

The SQQNN structure is characterized by the product of the matrices representing each of the K sequentially connected neurons. Since each neuron facilitates an arbitrary 1-qubit rotation, the cumulative effect of combining K neurons is equivalent to a single, effective quantum neuron, as follows:

$$\mathcal{N}_{\text{effective}} = \mathcal{N}_K \cdots \mathcal{N}_2 \mathcal{N}_1.$$

By employing multiple neurons, the model gains flexibility, increasing the model's expressive power and enhancing its ability to capture complex patterns in the data.

In this design, the angles α_k, β_k , and γ_k are determined by arbitrary functions applied to the input data. By composing these functions across multiple neurons, we significantly expand the SQQNN's degrees of freedom and enhance its capacity to adapt to the data during training. Thus, for any function defining the angles in a single-neuron SQQNN, there exists an inverse process and a corresponding set of functions for defining the angles in a multi-neuron SQQNN. This method provides a structured approach to enhance the flexibility of single-neuron SQQNNs, allowing for greater adaptability and improved training outcomes.

The circuit of the network is parameterized by the set of angles $\{\alpha_k, \beta_k, \gamma_k, \theta_k, \omega_k\}$. Let Ω_k denote one of the model's parameters associated with \mathcal{N}_k . To implement the learning algorithm,

we consider Ω_k as a function from \mathbb{R}^p to \mathbb{R} , representing a trainable weighted function typically derived from dataset inputs. To work with the effective neuron, we extend the function used by a single-neuron model to an effective function $\Omega(x)$, defined as

$$\Omega(x_i) = c_0 + \sum_{k=1}^K \sum_{j=1}^p c_{kj} x_{ij}^k, \quad (7)$$

where c_{kj} represents the unknown coefficients to be determined during training; K indicates the number of power terms, interpreted as the number of neurons; and x_{ij} is the j -th component of dataset instance x_i , which has p dimensions. The argument of $\Omega(x)$ can be an arbitrary vector x in \mathbb{R}^p . Although Eq. (7) is a specific choice, alternative formulations are possible. This choice draws inspiration from the Taylor series, allowing for a more precise approximation of any analytical function through polynomial terms, thereby enhancing the model’s expressiveness. It is also derived from a simplified version of the network, where the parameters formally sum up, resulting in Eq. (7).

We propose a reduced SQQNN defined by using the reduced neuron with the activation function (6) as illustrated in Fig. 2. In this setup, the network’s circuit comprises a sequence of $R_y(\beta_k)$ rotations, each parameterized by angle $\Omega_k = \beta_k$, defined as

$$\beta_k(x_i) = c_0 \delta_{k1} + \sum_{j=1}^p c_{kj} x_{ij}^k, \quad (8)$$

where δ is the Kronecker delta. The network is depicted in Fig. 4. The collective effect of all neurons is equivalent to a single $R_y(\beta)$ rotation, where all angles are summed as $\beta = \sum_{k=1}^K \beta_k$, leading to Eq. (7). Consequently, the SQQNN model simplifies to the circuit proposed in Fig. 2.

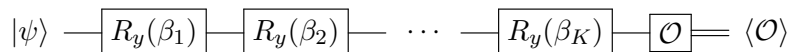


Figure 4: Representation of the reduced SQQNN. Each neuron \mathcal{N}_k is the rotation operator $R_y(\beta_k)$, which has only one trainable parameter.

Our proposal differs from Ref. [34] in at least two key aspects. First, in Ref. [34], the input data are directly used as the arguments of three-parameter unitary gates, requiring no classical pre-processing when the data have exactly three dimensions. In contrast, our approach can handle input data with any number of dimensions, but it requires classical pre-processing to compute the final values of the angles used as arguments for the rotation gates. Second, the algebraic operation intrinsic to the model in Ref. [34] is the Hadamard product between the weights and the input data, whereas in our approach, a single neuron computes the dot product between the weights and the input data. For architectures involving multiple neurons, the dot product extends to the weights and the powers of the input data entries.

We consistently use the function format described by Eq. (7) when training the SQQNNs in the applications presented below. In Sections 5.1 and 5, we set $K = 1$, indicating that $\beta(x_i) = c_0 + \sum_{j=1}^p c_j x_{ij}$ is sufficient to achieve accurate results for regression tasks. In contrast, for Section 6, we use $K \geq 1$ to demonstrate error reduction.

4. Training Methods

In machine learning, training refers to the process through which a model improves its performance on a specific task by identifying patterns within a dataset. This improvement is typically achieved by optimizing a set of weights, $(c_0, \dots, c_p) \in \mathbb{R}^{p+1}$, with the goal of minimizing the loss function. This function quantifies the discrepancy between the model's predictions and the actual outcomes. Throughout training, the model iteratively adjusts its parameters based on feedback from the loss function, gradually reducing errors and enhancing predictive accuracy. This process is generally carried out through gradient descent, which incrementally refines the model's parameters by following the gradient of the loss function, or via other optimization algorithms described later. The ultimate goal of learning is to enable the model to generalize well, not only on the training data but also on new, unseen data, by capturing essential patterns and relationships within the dataset.

For regression tasks, we use the Mean Square Error (MSE) loss function

$$\text{MSE}(\Omega, \mathbb{D}) = \frac{1}{n} \sum_{i=1}^n (\hat{y}_i - y_i)^2, \quad (9)$$

and for classification tasks, we use the hinge loss function

$$\text{Hinge}(\Omega, \mathbb{D}) = \frac{1}{n} \sum_{i=1}^n \max\{0, 1 - \hat{y}_i y_i\}, \quad (10)$$

where \hat{y}_i is the model's estimated output when the input is the dataset element x_i . The estimated output \hat{y}_i is calculated using Eq. (4). With ϕ and φ set to 0, the model's output is defined as follows

$$\begin{aligned} \hat{y} = & \cos \beta \cos \theta \cos \omega - \cos \alpha \sin \beta \sin \theta \cos \omega - \sin \beta \cos \gamma \cos \theta \sin \omega + \\ & \sin \alpha \sin \gamma \sin \theta \sin \omega - \cos \alpha \cos \beta \cos \gamma \sin \theta \sin \omega. \end{aligned} \quad (11)$$

The angles α , β , γ , θ , and ω are estimated based on the weights and input data. The loss function can be minimized with respect to the weights using standard methods such as the gradient descent method.

4.1. Gradient Descent

The primary concept of gradient descent is to iteratively adjust the model parameters in the opposite direction of the gradient of the loss function. Initially, the model parameters are set randomly. In each iteration, the gradient of the loss function with respect to the parameters is computed. The parameters are then updated by a factor controlled by the learning rate (η), as shown in the following equation:

$$\Omega_{t+1} = \Omega_t - \eta \nabla_{\Omega} \text{Loss}(\Omega_t, \mathbb{D}). \quad (12)$$

This process continues until the loss function reaches a sufficiently low value or until the gradient approaches zero, indicating that a minimum has been reached. The advantages of using gradient descent include simplicity of the model, efficiency, and adaptability to high-dimensional data. However, it can become trapped in local minima. It is important to choose a learning rate that ensures effective convergence.

To apply the gradient descent method for the single-qubit case, it is necessary to calculate the gradient of the loss function with respect to the angles α , β , γ , θ , and ω . Eventually, we analytically compute the partial derivatives of \hat{y} (Eq. (11)) with respect to these angles, which simplifies the training process. The expressions for these derivatives are

$$\begin{aligned}
\partial\hat{y}/\partial\alpha &= \sin\alpha\sin\beta\sin\theta\cos\omega + \cos\alpha\sin\gamma\sin\theta\sin\omega + \sin\alpha\cos\beta\cos\gamma\sin\theta\sin\omega; \\
\partial\hat{y}/\partial\beta &= -\sin\beta\cos\theta\cos\omega - \cos\alpha\cos\beta\sin\theta\cos\omega - \cos\beta\cos\gamma\cos\theta\sin\omega + \\
&\quad \cos\alpha\sin\beta\cos\gamma\sin\theta\sin\omega; \\
\partial\hat{y}/\partial\gamma &= \sin\beta\sin\gamma\cos\theta\sin\omega + \sin\alpha\cos\gamma\sin\theta\sin\omega + \cos\alpha\cos\beta\sin\gamma\sin\theta\sin\omega; \\
\partial\hat{y}/\partial\theta &= -\cos\beta\sin\theta\cos\omega - \cos\alpha\sin\beta\cos\theta\cos\omega + \sin\beta\cos\gamma\sin\theta\sin\omega + \\
&\quad \sin\alpha\sin\gamma\cos\theta\sin\omega - \cos\alpha\cos\beta\cos\gamma\cos\theta\sin\omega; \\
\partial\hat{y}/\partial\omega &= -\cos\beta\cos\theta\sin\omega + \cos\alpha\sin\beta\sin\theta\sin\omega - \sin\beta\cos\gamma\cos\theta\cos\omega + \\
&\quad \sin\alpha\sin\gamma\sin\theta\cos\omega - \cos\alpha\cos\beta\cos\gamma\sin\theta\cos\omega.
\end{aligned}$$

4.2. Polynomial-based Linear Least Squares

In this subsection, we introduce a training algorithm specifically designed for binary classification tasks using reduced SQQNNs, based on successive powers of the entries of the dataset elements. The function mapping data to the angle β is defined as

$$\beta(x) = \arccos \left[\tanh \left(c_0 + \sum_{k=1}^K \sum_{j=1}^p c_{kj} x_{ij}^k \right) \right]. \quad (13)$$

Substituting this function into Eq. (6) yields

$$\operatorname{arctanh}(y'_i) = c_0 + \sum_{k=1}^K \sum_{j=1}^p c_{kj} x_{ij}^k, \quad (14)$$

where $y'_i = -1 + \epsilon$ if $y_i = -1$, $y'_i = 1 - \epsilon$ if $y_i = 1$, and $y'_i = y_i$ otherwise. The small parameter $\epsilon > 0$ is introduced because the \tanh function never reaches -1 or 1, necessitating the adjustment of y_i by this parameter. Typically, in applications, we set $\epsilon = 10^{-16}$.

The coefficients c_0 and c_{kj} are determined using the least squares linear regression formula

$$S = (X^T X)^+ X^T Y, \quad (15)$$

where S is the vector of coefficients

$$S = [c_0 \quad c_{11} \quad \cdots \quad c_{1p} \quad \cdots \quad c_{1K} \quad \cdots \quad c_{1K}]^T,$$

Y is the label vector modified by the $\operatorname{arctanh}$ function

$$Y = [\operatorname{arctanh}(y'_1) \quad \operatorname{arctanh}(y'_2) \quad \cdots \quad \operatorname{arctanh}(y'_n)]^T,$$

and X is a matrix constructed from the dataset inputs

$$X = \begin{bmatrix} 1 & x_{11} & \cdots & x_{1p} & \cdots & x_{11}^k & \cdots & x_{1p}^k & \cdots & x_{11}^K & \cdots & x_{1p}^K \\ \vdots & \vdots & \vdots & \vdots & \vdots & \vdots & \vdots & \vdots & \vdots & \vdots & \vdots & \vdots \\ 1 & x_{i1} & \cdots & x_{ip} & \cdots & x_{i1}^k & \cdots & x_{ip}^k & \cdots & x_{i1}^K & \cdots & x_{ip}^K \\ \vdots & \vdots & \vdots & \vdots & \vdots & \vdots & \vdots & \vdots & \vdots & \vdots & \vdots & \vdots \\ 1 & x_{n1} & \cdots & x_{np} & \cdots & x_{n1}^k & \cdots & x_{np}^k & \cdots & x_{n1}^K & \cdots & x_{np}^K \end{bmatrix}.$$

X includes not only the raw dataset inputs but also the successive powers of their entries up to degree K , enabling the model to capture higher-order relationships in the data.

In this formulation, X^T represents the transpose of the matrix X , and $(X^T X)^+$ denotes the inverse or Moore-Penrose pseudo-inverse of the matrix $X^T X$. This approach allows for the efficient determination of network parameters in a single step, significantly accelerating the training process. It is important to note that, at the end of the training, one of the global minima is achieved.

5. Regression Evaluation

In this section, we evaluate the effectiveness of SQQNN in performing regression tasks. Regression is a critical application for quantum neural networks as it requires accurately modeling continuous relationships and predicting real-valued outputs, which were initially rescaled to the range $[-1, 1]$ and subsequently recalibrated to their original range. We apply SQQNN to three types of regression tasks: logic gates, modeling continuous functions, and analyzing real-world datasets. By assessing its performance in these cases, we aim to demonstrate SQQNN’s precision and adaptability in diverse regression scenarios, using the gradient descent method. For the real-world datasets, we employed 10-fold cross-validation to ensure robust evaluation.

5.1. Logic Gate Evaluation

The results of training the SQQNN to evaluate logical gates are shown in Table 1. Here, we present the training error and the number of gradient descent epochs required for each gate, including AND, OR, XOR, NAND, NOR, and XNOR. The SQQNN was trained with a single neuron ($K = 1$).

Gate	MSE	Epochs	Gate	MSE	Epochs
AND	$9 \cdot 10^{-4}$	38	NAND	$2 \cdot 10^{-3}$	61
OR	$2 \cdot 10^{-4}$	64	NOR	$2 \cdot 10^{-3}$	75
XOR	$1 \cdot 10^{-3}$	79	XNOR	$6 \cdot 10^{-4}$	47

Table 1: Experimental results of training the SQQNN on logical gates using gradient descent.

Table 1 shows that SQQNN achieved low training errors across all gates, indicating effective error minimization. The number of gradient descent iterations also remained relatively low across all logical gates, including more complex, nonlinear ones such as XOR and XNOR. These results highlight the SQQNN’s ability to learn efficiently across various logical functions, demonstrating its flexibility in capturing both linear and non-linear behavior in binary logic operations.

Ref. [43] analyzed logic gates using two-qubit QNNs and reported that the QNN achieved less than 1% error within a single epoch. Our experiments indicate that the SQQNN requires at least 5 epochs to reach an error rate below 1%. However, the classical networks analyzed in Ref. [43] required significantly more epochs to achieve a 1% error rate, far exceeding the performance summarized in Table 1, which shows a much smaller error. This comparison suggests that, for certain regression tasks, two-qubit QNNs may train faster than single-qubit QNNs.

5.2. Sinc function

The sinc function, defined as

$$\text{sinc}(x) = \frac{\sin(x)}{x}, \quad (16)$$

is a standard benchmark for regression tasks due to its oscillatory, non-linear nature and decaying amplitude, which present challenges for models to accurately capture without overfitting. For this experiment, we generated data based on the sinc function and trained SQQNNs with a single neuron to predict previously unseen data points. The dataset consisted of 800 data points for training, 100 for validation, and 100 for testing.

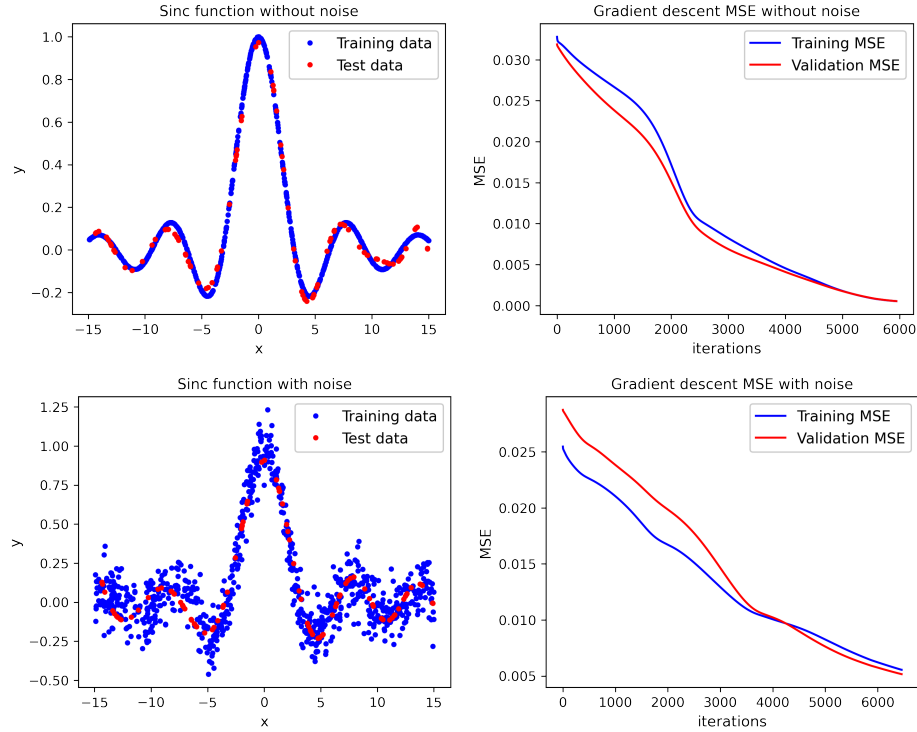


Figure 5: Performance of the SQQNN on a sinc function regression task using a single neuron. The top-left panel shows the noiseless training and test data combined, while the bottom-left panel displays the results with added white noise. The top-right and bottom-right panels depict the corresponding error as a function of the number of iterations.

Figure 5 illustrates the performance of the SQQNN on this task under two scenarios: training with noiseless data and training with data affected by white noise with standard deviation of 0.01. In the top-left panel, the training and test datasets for the noiseless case are shown, clearly aligning with the sinc function, while the corresponding mean squared error, plotted as a function of iterations in the top-right panel, converges to approximately 10^{-3} after $7 \cdot 10^4$ iterations. Similarly, the bottom-left panel shows the training and test datasets when noise is added to the data, with the SQQNN successfully approximating the sinc function despite the noise. The bottom-right panel demonstrates that the error decreases at a comparable rate, even with noisy training data. These results highlight the SQQNN’s robustness and ability to handle both clean and noisy regression tasks effectively.

5.3. Combined Cycle Power Plant Dataset

The Combined Cycle Power Plant (CCPP) dataset, sourced from the UCI Machine Learning Repository¹, provides 9,568 samples of data collected from a gas turbine under full load conditions. It features four input variables—ambient temperature, ambient pressure, relative humidity, and exhaust vacuum—and one target variable, the net electrical energy output of the plant, measured in megawatts. The dataset is widely used for regression tasks due to its smooth, non-linear relationships and strong correlations between features and the target variable. With its clean and comprehensive structure, the CCPP dataset serves as a valuable benchmark for modeling and predicting energy production under varying environmental and operational conditions.

<i>K</i> Neurons	Training MSE	Validation MSE	Test MSE
1	0.0059 ± 0.0008	0.0059 ± 0.0008	0.0059 ± 0.0007
2	0.0045 ± 0.0005	0.0048 ± 0.0006	0.0045 ± 0.0005
3	0.0040 ± 0.0002	0.0043 ± 0.0003	0.0040 ± 0.0004
4	0.0037 ± 0.0002	0.0042 ± 0.0003	0.0037 ± 0.0003
5	0.0038 ± 0.0004	0.0043 ± 0.0004	0.0039 ± 0.0004
6	0.0035 ± 0.0002	0.0040 ± 0.0003	0.0035 ± 0.0002

Table 2: Performance metrics (MSE for training, validation, and test) for the combined cycle power plant dataset as the numbers of neurons K increases.

Table 2 presents the performance of the model on the Combined Cycle Power Plant dataset as the number of neurons (K) increases. The results demonstrate a clear improvement in MSE across training, validation, and test sets as K increases up to 6, with the test MSE decreasing from 0.0059 ± 0.0007 for $K = 1$ to 0.0035 ± 0.0002 for $K = 6$. This indicates that increasing the network complexity enhances the model’s ability to capture the non-linear relationships within the dataset. Notably, the small variances in MSE values suggest that the model maintains stable and consistent performance across different subsets of the data, showcasing its robustness for this regression task.

Ref. [40] reported training and test MSE values of 0.048 ± 0.0001 and 0.051 ± 0.0003 , respectively, based on 30 experiments with state preparation. In contrast, our results were approximately ten times lower, demonstrating a significant improvement.

5.4. Communities and Crime Dataset

The Communities and Crime dataset, sourced from the UCI Machine Learning Repository², provides comprehensive data on crime rates across 1,994 U.S. communities, alongside key socio-economic and demographic factors. The dataset focuses on various types of crimes, including violent offenses such as murder, rape, robbery, and assault, as well as property crimes like burglary, theft, and motor vehicle theft. Its target variable is the violent crime rate per capita, making it particularly suitable for regression analysis. In addition to crime statistics, the dataset includes socio-economic variables such as population size, income levels, education attainment, poverty rates, and the proportion of minority populations. With its combination of detailed crime metrics and contextual information, this dataset enables an in-depth exploration of the

¹<https://archive.ics.uci.edu/dataset/294/combined+cycle+power+plant>

²<https://archive.ics.uci.edu/dataset/183/communities+and+crime>

relationships between community characteristics and crime rates, as well as regional variations in crime patterns. This dataset was used in many papers [44, 45, 46].

K Neurons	Training MSE	Validation MSE	Test MSE
1	0.0426 ± 0.0111	0.0405 ± 0.0110	0.0434 ± 0.0133
2	0.0522 ± 0.0099	0.0561 ± 0.0151	0.0539 ± 0.0154
3	0.0604 ± 0.0239	0.0613 ± 0.0260	0.0600 ± 0.0235
4	0.0733 ± 0.0203	0.0842 ± 0.0298	0.0804 ± 0.0235
5	0.0853 ± 0.0227	0.0833 ± 0.0274	0.0853 ± 0.0225
6	0.1168 ± 0.0242	0.1234 ± 0.0202	0.1195 ± 0.0252

Table 3: Performance metrics for the communities and crime dataset as the numbers of neurons K increases.

Table 3 summarizes the performance of SQQNN on the Communities and Crime dataset for varying numbers of neurons (K). The results indicate that the training, validation, and test Mean Squared Errors (MSE) increase as K grows, with the lowest MSE observed for $K = 1$ (training MSE: 0.0426 ± 0.0111 , test MSE: 0.0434 ± 0.0133). This trend suggests that increasing the network’s complexity may lead to overfitting, as the gap between training and validation errors becomes more pronounced for larger K . The relatively small variances in MSE values across all configurations highlight the stability of the model, but the overall performance diminishes as the network size grows, pointing to the suitability of smaller models for this dataset. These results underscore the importance of balancing model complexity and dataset size to avoid overfitting.

Ref. [46] modeled this dataset using classical methods and reported a training MSE of 0.299. In comparison, our results are significantly lower, underscoring the superior learning capability of our network.

6. Classification Evaluation

In this section, we present the results of the SQQNN architecture, evaluated on both synthetic and real datasets to demonstrate its effectiveness and versatility in various binary classification tasks. The training method employed is the polynomial-based linear least squares. For the analysis of real datasets, we employed accuracy, precision, sensitivity, specificity, and F1 score to evaluate the classification performance. The output classes used 1 and -1 to represent each category. Additionally, 10-fold cross-validation was applied to ensure robust evaluation of the real datasets.

6.1. Two Moons Dataset

The Two Moons dataset is a synthetic dataset commonly used for testing classification models. It consists of two interlocking half-moon shapes that are challenging to separate linearly, making it an ideal benchmark for assessing the capabilities of nonlinear classifiers. For this experiment, the dataset was generated with a noise parameter set to 0.07, the training set comprised 1,000 data points and test set with 100 samples.

The results in Table 4 highlight the model’s high performance. The classification achieved accuracy, precision, sensitivity, and F1-score of 1 across the board, indicating that the model fully captured the underlying structure of the data. In this application, two neurons are sufficient to achieve high accuracy. Fig. 6 illustrates this progression, showing a significant improvement in classification accuracy with additional neurons. The SQQNN quickly adapts to fit all synthetic data points, demonstrating its ability to effectively classify complex, nonlinearly separable data.

K Neurons	Accuracy	Precision	Sensitivity	Specificity	F1 Score
1	0.87	0.8776	0.86	0.88	0.8687
2	0.99	0.9804	1.0	0.98	0.9901
3	0.99	0.9804	1.0	0.98	0.9901
4	1.0	1.0	1.0	1.0	1.0
5	1.0	1.0	1.0	1.0	1.0
6	1.0	1.0	1.0	1.0	1.0

Table 4: Performance metrics for the Two Moons dataset as the numbers of neurons K increases.

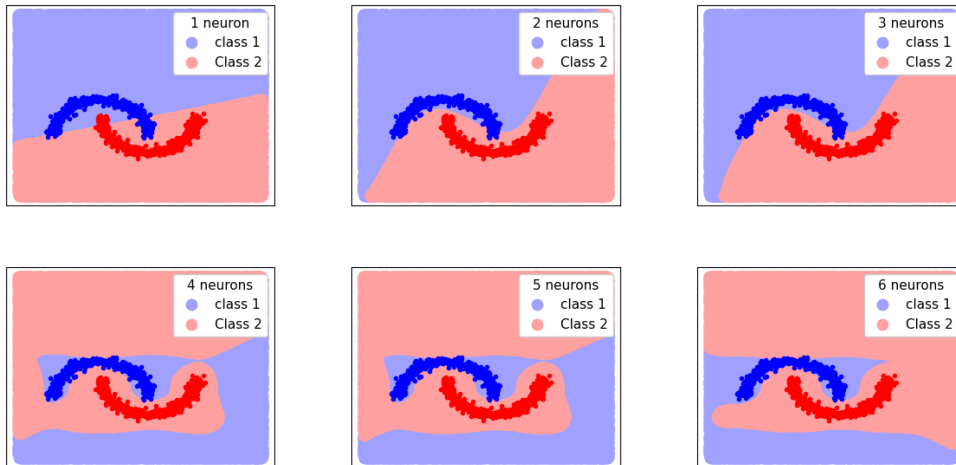


Figure 6: Decision boundaries of the SQNN classifier with 1 to 6 neurons, trained on the two-dimensional, nonlinearly separable Two Moons dataset.

6.2. Wisconsin Breast Cancer Dataset

The Wisconsin Breast Cancer Dataset (WBCD), sourced from the UCI Machine Learning Repository³, is a widely recognized benchmark in medical diagnostics and machine learning research. This dataset comprises 569 samples, each characterized by 30 numeric features derived from fine needle aspiration (FNA) tests of breast tissue. The features capture various morphological properties of cell nuclei, including radius, texture, perimeter, area, and smoothness, among others. These descriptors enable the differentiation between benign and malignant tumors, facilitating accurate diagnostic predictions. The WBCD serves as a critical testbed for evaluating the performance of classification algorithms, offering a well-balanced distribution of classes and a real-world application of machine learning in healthcare.

The results presented in Table 5 were produced using the SQNN architecture, with the model parameter K increased from 1 to 10. This adjustment was made to enhance the network’s capacity and improve classification accuracy. By progressively increasing K , we evaluated the relationship between model complexity and performance, leveraging the WBCD dataset to validate the effectiveness of SQNN in reducing classification errors.

Despite fluctuations in all performance measures, Table 5 highlights a clear trend toward

³<https://archive.ics.uci.edu/dataset/15/breast+cancer+wisconsin+original>

K Neurons	Accuracy (\pm)	Precision (\pm)	Sensitivity (\pm)	Specificity (\pm)	F1 (\pm)
1	0.951 \pm 0.025	0.994 \pm 0.017	0.878 \pm 0.068	0.878 \pm 0.068	0.931 \pm 0.034
2	0.954 \pm 0.020	1.000 \pm 0.000	0.879 \pm 0.047	0.879 \pm 0.047	0.935 \pm 0.027
3	0.954 \pm 0.021	1.000 \pm 0.000	0.880 \pm 0.050	0.880 \pm 0.050	0.935 \pm 0.029
4	0.956 \pm 0.023	0.988 \pm 0.024	0.894 \pm 0.052	0.894 \pm 0.052	0.938 \pm 0.034
5	0.954 \pm 0.027	0.988 \pm 0.025	0.890 \pm 0.054	0.890 \pm 0.054	0.936 \pm 0.039
6	0.956 \pm 0.032	0.987 \pm 0.026	0.896 \pm 0.074	0.896 \pm 0.074	0.938 \pm 0.050
7	0.949 \pm 0.030	0.982 \pm 0.028	0.882 \pm 0.072	0.882 \pm 0.072	0.928 \pm 0.045
8	0.958 \pm 0.028	0.982 \pm 0.028	0.905 \pm 0.066	0.905 \pm 0.066	0.941 \pm 0.042
9	0.958 \pm 0.028	0.982 \pm 0.028	0.905 \pm 0.066	0.905 \pm 0.066	0.941 \pm 0.042
10	0.956 \pm 0.028	0.982 \pm 0.028	0.901 \pm 0.066	0.901 \pm 0.066	0.938 \pm 0.041

Table 5: Performance metrics for the WBCD dataset as the number of neurons K increases.

improvement as the number of neurons increases, indicating the model’s growing ability to accurately distinguish between classes. The consistently low variance across all metrics further highlights the robustness of SQQNN, even with a larger number of neurons. Notably, increasing K beyond 8 leads to diminishing returns, suggesting that the model reaches optimal performance with a moderate number of neurons while maintaining computational efficiency.

Ref. [39] reported a validation accuracy of 0.94 ± 0.024 using a bagging ensemble with a quantum asymptotically universal multi-feature approach. This result is statistically comparable to our findings.

6.3. MNIST Dataset

The MNIST dataset, a standard benchmark in the field of machine learning, consists of 70,000 grayscale images of handwritten digits, partitioned into 60,000 training samples and 10,000 test samples. Each image, represented as a 28×28 pixel grid, encapsulates the complexity of real-world digit recognition tasks while maintaining computational simplicity. Despite its relative simplicity, MNIST remains a critical testbed for evaluating novel neural network architectures. In this work, we use MNIST to show the performance and generalization potential of the SQQNN architecture, establishing a baseline for its capabilities in image recognition tasks. To achieve this, we applied the Discrete Cosine Transform (DCT) [47] to the images as a pre-processing step.



Figure 7: Examples of digits from the MNIST dataset incorrectly predicted.

Fig. 7 depicts sample digits from 0 to 9 from the MNIST dataset that were incorrectly predicted, highlighting the variability in handwriting styles and pixel intensity. The results presented in Table 6 were produced using $K = 1$ and the reduced version of SQQNN, specifically designed to optimize computational efficiency while maintaining high classification accuracy. The reduced model was trained using the polynomial-based linear least squares method, leveraging the MNIST training set for evaluation. Each training iteration took approximately 8 seconds on a DELL Vostro 3480 notebook with an Intel Core i5-8265U 1.60GHz x8 CPU, 8GB DDR4 RAM, and Ubuntu 22.04.4 LTS.

The results presented in Table 6 demonstrate the remarkable performance of the SQQNN architecture across various MNIST class pairings, achieving near-perfect accuracy, precision, sensitivity, specificity, and F1 scores in most cases. For simpler pairings, such as digits 0 and 1, the network attained an accuracy of 0.999 ± 0.001 , reflecting its ability to distinguish visually

Classes	Accuracy	Precision	Sensitivity	Specificity	F1
0 and 1	0.999 ± 0.001	0.999 ± 0.001	0.999 ± 0.001	0.999 ± 0.001	0.999 ± 0.001
0 and 2	0.995 ± 0.002	0.996 ± 0.002	0.994 ± 0.002	0.994 ± 0.002	0.995 ± 0.002
0 and 3	0.997 ± 0.002	0.997 ± 0.002	0.997 ± 0.003	0.997 ± 0.003	0.997 ± 0.002
0 and 4	0.997 ± 0.001	0.996 ± 0.002	0.997 ± 0.002	0.997 ± 0.002	0.997 ± 0.001
0 and 5	0.995 ± 0.002	0.995 ± 0.003	0.995 ± 0.002	0.995 ± 0.002	0.995 ± 0.002
0 and 6	0.993 ± 0.002	0.993 ± 0.003	0.993 ± 0.002	0.993 ± 0.002	0.993 ± 0.002
0 and 7	0.997 ± 0.001	0.996 ± 0.003	0.998 ± 0.002	0.998 ± 0.002	0.997 ± 0.001
0 and 8	0.995 ± 0.002	0.996 ± 0.003	0.994 ± 0.003	0.994 ± 0.003	0.995 ± 0.002
0 and 9	0.993 ± 0.003	0.995 ± 0.002	0.992 ± 0.004	0.992 ± 0.004	0.993 ± 0.003
1 and 2	0.992 ± 0.002	0.991 ± 0.003	0.993 ± 0.003	0.993 ± 0.003	0.992 ± 0.002
1 and 3	0.994 ± 0.002	0.994 ± 0.004	0.994 ± 0.003	0.994 ± 0.003	0.994 ± 0.002
1 and 4	0.997 ± 0.001	0.996 ± 0.002	0.996 ± 0.002	0.996 ± 0.002	0.996 ± 0.001
1 and 5	0.995 ± 0.001	0.995 ± 0.002	0.994 ± 0.003	0.994 ± 0.003	0.995 ± 0.001
1 and 6	0.998 ± 0.002	0.998 ± 0.002	0.997 ± 0.003	0.997 ± 0.003	0.997 ± 0.002
1 and 7	0.994 ± 0.003	0.994 ± 0.003	0.992 ± 0.004	0.992 ± 0.004	0.993 ± 0.003
1 and 8	0.994 ± 0.003	0.994 ± 0.004	0.993 ± 0.004	0.993 ± 0.004	0.993 ± 0.003
1 and 9	0.995 ± 0.001	0.995 ± 0.003	0.995 ± 0.002	0.995 ± 0.002	0.995 ± 0.001
2 and 3	0.976 ± 0.004	0.983 ± 0.004	0.968 ± 0.007	0.968 ± 0.007	0.976 ± 0.004
2 and 4	0.994 ± 0.002	0.992 ± 0.003	0.996 ± 0.002	0.996 ± 0.002	0.994 ± 0.002
2 and 5	0.980 ± 0.003	0.979 ± 0.004	0.980 ± 0.005	0.980 ± 0.005	0.979 ± 0.003
2 and 6	0.988 ± 0.002	0.986 ± 0.005	0.991 ± 0.003	0.991 ± 0.003	0.988 ± 0.003
2 and 7	0.986 ± 0.002	0.988 ± 0.004	0.985 ± 0.004	0.985 ± 0.004	0.987 ± 0.002
2 and 8	0.980 ± 0.003	0.977 ± 0.004	0.983 ± 0.004	0.983 ± 0.004	0.980 ± 0.004
2 and 9	0.990 ± 0.002	0.988 ± 0.004	0.992 ± 0.004	0.992 ± 0.004	0.990 ± 0.003
3 and 4	0.998 ± 0.001	0.997 ± 0.002	0.999 ± 0.001	0.999 ± 0.001	0.998 ± 0.001
3 and 5	0.966 ± 0.003	0.969 ± 0.006	0.957 ± 0.003	0.957 ± 0.003	0.963 ± 0.003
3 and 6	0.997 ± 0.001	0.997 ± 0.002	0.997 ± 0.002	0.997 ± 0.002	0.997 ± 0.001
3 and 7	0.991 ± 0.002	0.989 ± 0.004	0.995 ± 0.002	0.995 ± 0.002	0.992 ± 0.002
3 and 8	0.985 ± 0.002	0.982 ± 0.003	0.988 ± 0.003	0.988 ± 0.003	0.985 ± 0.002
3 and 9	0.990 ± 0.002	0.991 ± 0.003	0.988 ± 0.003	0.988 ± 0.003	0.989 ± 0.002
4 and 5	0.997 ± 0.001	0.998 ± 0.002	0.996 ± 0.002	0.996 ± 0.002	0.997 ± 0.001
4 and 6	0.993 ± 0.003	0.994 ± 0.003	0.992 ± 0.003	0.992 ± 0.003	0.993 ± 0.003
4 and 7	0.990 ± 0.003	0.993 ± 0.002	0.988 ± 0.004	0.988 ± 0.004	0.990 ± 0.003
4 and 8	0.994 ± 0.002	0.997 ± 0.003	0.991 ± 0.004	0.991 ± 0.004	0.994 ± 0.003
4 and 9	0.978 ± 0.004	0.979 ± 0.005	0.977 ± 0.005	0.977 ± 0.005	0.978 ± 0.004
5 and 6	0.989 ± 0.003	0.988 ± 0.005	0.991 ± 0.003	0.991 ± 0.003	0.989 ± 0.003
5 and 7	0.995 ± 0.001	0.995 ± 0.002	0.997 ± 0.002	0.997 ± 0.002	0.996 ± 0.001
5 and 8	0.989 ± 0.003	0.992 ± 0.003	0.987 ± 0.005	0.987 ± 0.005	0.989 ± 0.003
5 and 9	0.988 ± 0.003	0.991 ± 0.004	0.987 ± 0.006	0.987 ± 0.006	0.989 ± 0.003
6 and 7	0.998 ± 0.001	0.998 ± 0.002	0.998 ± 0.001	0.998 ± 0.001	0.998 ± 0.001
6 and 8	0.988 ± 0.002	0.989 ± 0.004	0.987 ± 0.005	0.987 ± 0.005	0.988 ± 0.002
6 and 9	0.995 ± 0.001	0.996 ± 0.002	0.995 ± 0.002	0.995 ± 0.002	0.995 ± 0.001
7 and 8	0.995 ± 0.002	0.997 ± 0.003	0.993 ± 0.002	0.993 ± 0.002	0.995 ± 0.002
7 and 9	0.971 ± 0.004	0.961 ± 0.004	0.980 ± 0.006	0.980 ± 0.006	0.970 ± 0.005
8 and 9	0.985 ± 0.003	0.989 ± 0.003	0.982 ± 0.004	0.982 ± 0.004	0.985 ± 0.003

Table 6: MNIST performance metrics for all class pairings using a single neuron ($K = 1$).

distinct classes with minimal error. Even for more challenging combinations, such as 2 and 3 or 7 and 9, the accuracy remained high, at 0.976 ± 0.004 and 0.971 ± 0.004 , respectively, underscoring the robustness of the reduced SQQNN model. The consistently low variance across all metrics indicates stable performance.

Ref. [18] achieved an accuracy of 0.98 for digits 0 and 1. In comparison, our approach improved the results to 0.999. Similarly, Ref. [39] reported a validation accuracy of 0.949 ± 0.024 for digits 8 and 9 using a bagging ensemble with a quantum asymptotically universal multi-feature approach. In contrast, our method achieved significantly better performance, with an accuracy of approximately 0.985. These results highlight the reliability and precision of our network in performing binary classification tasks on the MNIST dataset.

Ref. [9] compared the performance of classical and quantum machine learning methods across

various datasets, including MNIST. The study found that classical models generally outperformed quantum classifiers. Specifically, for the MNIST dataset, the Classical Multi-Layer Perceptron (MLP) classifier, augmented by pre-processing techniques such as resolution reduction and Principal Component Analysis (PCA), achieved superior performance with an accuracy close to 1, comparable to the results obtained by the SQQNN.

7. Final remarks

We use a Single-Qubit Quantum Neural Network (SQQNN), a quantum machine learning framework that leverages the simplicity and efficiency of single-qubit neurons. By employing parameterized single-qubit operations, the SQQNN offers a streamlined yet powerful architecture for both regression and binary classification tasks. This design significantly reduces hardware requirements, simplifies implementation, and is compatible with near-term quantum devices, making it a practical alternative to more complex multi-qubit approaches.

We validated the SQQNN’s capabilities through diverse applications. The model achieved near-zero training errors in logic gate evaluations, demonstrating its ability to handle linear and nonlinear relationships efficiently. For other regression tasks, the SQQNN successfully modeled continuous functions and real-world datasets, showcasing its adaptability and generalization. In classification tasks, increasing the number of neurons significantly reduced error, and the model performed strongly on both synthetic and real-world datasets, including MNIST. These results highlight the SQQNN’s scalability and flexibility.

To optimize the network, we employed two learning methods: gradient descent with iterative refinement for regression tasks and an improved global optimization approach using a matrix-based dataset representation called polynomial-based linear least squares (LLS) for classification tasks. The polynomial-based LLS method offers rapid results, and its use with a single neuron ($K = 1$) eliminates the need for deep learning architectures. This demonstrates an efficient and streamlined training approach, making it a valuable contribution to both quantum and classical machine learning. This combination of training methods ensures accurate results across various tasks, highlighting the SQQNN’s versatility in leveraging different optimization strategies tailored to specific problems.

The SQQNN provides a promising, efficient, and adaptable framework for practical quantum neural networks, bridging the gap between current quantum hardware and machine learning applications. Future research could explore extensions to multi-qubit systems, the development of novel activation functions, and the application of the model to diverse pattern datasets and real-world scenarios. Employing qudits for multi-ary classification, by capitalizing on the multi-output nature of quantum measurements, presents another intriguing direction.

Acknowledgements

The authors thank productive discussions with Dr. Adenilton J. da Silva and Professor Francesco Petruccione. The work of L. C. Souza was supported by CNPq grant number 302519/2024-6. The work of R. Portugal was supported by FAPERJ grant number CNE E-26/200.954/2022, and CNPq grant numbers 304645/2023-0 and 409552/2022-4.

Declaration of competing interest

The authors declare that they have no known competing financial interests or personal relationships that could have appeared to influence the work reported in this paper.

Data availability

Data are public.

References

- [1] W. S. McCulloch, W. Pitts, A logical calculus of the ideas immanent in nervous activity, *The Bulletin of Mathematical Biophysics* 5 (4) (1943) 115–133.
- [2] F. Rosenblatt, The perceptron: A probabilistic model for information storage and organization in the brain., *Psychological Review* 65 (6) (1958) 386–408. doi:10.1037/h0042519.
- [3] I. J. Goodfellow, Y. Bengio, A. Courville, *Deep Learning*, MIT Press, Cambridge, MA, USA, 2016, <http://www.deeplearningbook.org>.
- [4] D. A. Roberts, S. Yaida, *The Principles of Deep Learning Theory: An Effective Theory Approach to Understanding Neural Networks*, Cambridge University Press, Cambridge, 2022. doi:10.1017/9781009023405.
- [5] J. Biamonte, P. Wittek, N. Pancotti, P. Rebentrost, N. Wiebe, S. Lloyd, Quantum machine learning, *Nature* 549 (7671) (2017) 195–202. doi:10.1038/nature23474.
- [6] J. Liu, M. Liu, J.-P. Liu, Z. Ye, Y. Wang, Y. Alexeev, J. Eisert, L. Jiang, Towards provably efficient quantum algorithms for large-scale machine-learning models, *Nature Communications* 15 (1) (2024) 434. doi:10.1038/s41467-023-43957-x.
- [7] Y. Gujju, A. Matsuo, R. Raymond, Quantum machine learning on near-term quantum devices: Current state of supervised and unsupervised techniques for real-world applications, *Phys. Rev. Appl.* 21 (2024) 067001. doi:10.1103/PhysRevApplied.21.067001.
- [8] Y. Wang, J. Liu, A comprehensive review of quantum machine learning: from NISQ to fault tolerance, *Reports on Progress in Physics* 87 (11) (2024) 116402. doi:10.1088/1361-6633/ad7f69.
- [9] J. Bowles, S. Ahmed, M. Schuld, *Better than classical? The subtle art of benchmarking quantum machine learning models*, arXiv (2024) 2403.07059. URL <https://arxiv.org/abs/2403.07059>
- [10] M. Schuld, I. Sinayskiy, F. Petruccione, Simulating a perceptron on a quantum computer, *Physics Letters A* 379 (7) (2015) 660–663. doi:10.1016/j.physleta.2014.11.061.
- [11] N. Wiebe, A. Kapoor, K. M. Svore, Quantum perceptron models, in: *Proceedings of the 30th International Conference on Neural Information Processing Systems, NIPS’16*, Curran Associates Inc., Red Hook, NY, USA, 2016, p. 4006–4014.

- [12] A. J. da Silva, T. B. Ludermir, W. R. de Oliveira, Quantum perceptron over a field and neural network architecture selection in a quantum computer, *Neural Networks* 76 (2016) 55–64. [doi:10.1016/j.neunet.2016.01.002](https://doi.org/10.1016/j.neunet.2016.01.002).
- [13] K. H. Wan, O. Dahlsten, H. Kristjánsson, R. Gardner, M. S. Kim, Quantum generalisation of feedforward neural networks, *npj Quantum Information* 3 (1) (2017) 36. [doi:10.1038/s41534-017-0032-4](https://doi.org/10.1038/s41534-017-0032-4).
- [14] F. Tacchino, C. Macchiavello, D. Gerace, D. Bajoni, An artificial neuron implemented on an actual quantum processor, *npj Quantum Information* 5 (1) (2019) 26. [doi:10.1038/s41534-019-0140-4](https://doi.org/10.1038/s41534-019-0140-4).
- [15] M. Schuld, N. Killoran, Quantum machine learning in feature Hilbert spaces, *Phys. Rev. Lett.* 122 (2019) 040504. [doi:10.1103/PhysRevLett.122.040504](https://doi.org/10.1103/PhysRevLett.122.040504).
- [16] I. Cong, S. Choi, M. D. Lukin, Quantum convolutional neural networks, *Nature Physics* 15 (12) (2019) 1273–1278. [doi:10.1038/s41567-019-0648-8](https://doi.org/10.1038/s41567-019-0648-8).
- [17] M. Henderson, S. Shakya, S. Pradhan, T. Cook, Quantum convolutional neural networks: powering image recognition with quantum circuits, *Quantum Machine Intelligence* 2 (1) (2020) 2. [doi:10.1007/s42484-020-00012-y](https://doi.org/10.1007/s42484-020-00012-y).
- [18] S. Mangini, F. Tacchino, D. Gerace, C. Macchiavello, D. Bajoni, Quantum computing model of an artificial neuron with continuously valued input data, *Machine Learning: Science and Technology* 1 (4) (2020) 045008. [doi:10.1088/2632-2153/abaf98](https://doi.org/10.1088/2632-2153/abaf98).
- [19] D. Bokhan, A. S. Mastiukova, A. S. Boev, D. N. Trubnikov, A. K. Fedorov, Multiclass classification using quantum convolutional neural networks with hybrid quantum-classical learning, *Frontiers in Physics* 10 (2022). [doi:10.3389/fphy.2022.1069985](https://doi.org/10.3389/fphy.2022.1069985).
- [20] F. Benatti, G. Gramegna, S. Mancini, Pattern capacity of a single quantum perceptron, *Journal of Physics A: Mathematical and Theoretical* 55 (15) (2022) 155301. [doi:10.1088/1751-8121/ac58d1](https://doi.org/10.1088/1751-8121/ac58d1).
- [21] J. H. A. Carvalho, F. M. P. Neto, Parametrized constant-depth quantum neuron, *IEEE Transactions on Neural Networks and Learning Systems* 35 (11) (2024) 15932–15943. [doi:10.1109/TNNLS.2023.3290535](https://doi.org/10.1109/TNNLS.2023.3290535).
- [22] N. Kouda, N. Matsui, H. Nishimura, F. Peper, Qubit neural network and its learning efficiency, *Neural Computing & Applications* 14 (2) (2005) 114–121. [doi:10.1007/s00521-004-0446-8](https://doi.org/10.1007/s00521-004-0446-8).
- [23] E. Farhi, H. Neven, [Classification with quantum neural networks on near term processors](https://arxiv.org/abs/1802.06002), *ArXiv* (2018) 1802.06002.
URL <https://arxiv.org/abs/1802.06002>
- [24] M. Pechal, F. Roy, S. A. Wilkinson, G. Salis, M. Werninghaus, M. J. Hartmann, S. Filipp, Direct implementation of a perceptron in superconducting circuit quantum hardware, *Phys. Rev. Res.* 4 (2022) 033190. [doi:10.1103/PhysRevResearch.4.033190](https://doi.org/10.1103/PhysRevResearch.4.033190).

- [25] M. Schuld, F. Petruccione, *Supervised Learning with Quantum Computers*, Quantum Science and Technology, Springer, 2018. doi:10.1007/978-3-319-96424-9.
- [26] M. Schuld, F. Petruccione, *Machine Learning with Quantum Computers*, Quantum Science and Technology, Springer, Cham, 2021. doi:10.1007/978-3-030-83098-4.
- [27] S. Sim, P. D. Johnson, A. Aspuru-Guzik, Expressibility and entangling capability of parameterized quantum circuits for hybrid quantum-classical algorithms, *Advanced Quantum Technologies* 2 (12) (2019) 1900070. doi:10.1002/qute.201900070.
- [28] M. Benedetti, E. Lloyd, S. Sack, M. Fiorentini, Parameterized quantum circuits as machine learning models, *Quantum Science and Technology* 4 (4) (2019) 043001. doi:10.1088/2058-9565/ab4eb5.
- [29] X. Ding, Z. Song, J. Xu, Y. Hou, T. Yang, Z. Shan, Scalable parameterized quantum circuits classifier, *Scientific Reports* 14 (1) (2024) 15886. doi:10.1038/s41598-024-66394-2.
- [30] Y. Du, M.-H. Hsieh, T. Liu, D. Tao, Expressive power of parametrized quantum circuits, *Phys. Rev. Res.* 2 (2020) 033125. doi:10.1103/PhysRevResearch.2.033125.
- [31] M. Schuld, R. Sweke, J. J. Meyer, Effect of data encoding on the expressive power of variational quantum-machine-learning models, *Phys. Rev. A* 103 (2021) 032430. doi:10.1103/PhysRevA.103.032430.
- [32] R. Ghobadi, J. S. Oberoi, E. Zahedinejad, *The Power of One Qubit in Machine Learning*, arXiv (2019) 1905.01390.
URL <https://arxiv.org/pdf/1905.01390>
- [33] M. Karimi, A. Javadi-Abhari, C. Simon, R. Ghobadi, The power of one clean qubit in supervised machine learning, *Scientific Reports* 13 (1) (2023) 19975. doi:10.1038/s41598-023-46497-y.
- [34] A. Pérez-Salinas, A. Cervera-Lierta, E. Gil-Fuster, J. I. Latorre, Data re-uploading for a universal quantum classifier, *Quantum* 4 (2020) 226. doi:10.22331/q-2020-02-06-226.
- [35] A. Pérez-Salinas, D. López-Núñez, A. García-Sáez, P. Forn-Díaz, J. I. Latorre, One qubit as a universal approximant, *Phys. Rev. A* 104 (2021) 012405. doi:10.1103/PhysRevA.104.012405.
- [36] Z. Yu, H. Yao, M. Li, X. Wang, *Power and limitations of single-qubit native quantum neural networks*, in: A. H. Oh, A. Agarwal, D. Belgrave, K. Cho (Eds.), *Advances in Neural Information Processing Systems*, 2022.
URL <https://openreview.net/forum?id=XNjCGDr8N-W>
- [37] E. P. Tapia, G. Scarpa, A. Pozas-Kerstjens, A didactic approach to quantum machine learning with a single qubit, *Physica Scripta* 98 (5) (2023) 054001. doi:10.1088/1402-4896/acc5b8.
- [38] P. Easom-McCaldin, A. Bouridane, A. Belatreche, R. Jiang, S. Al-Maadeed, Efficient quantum image classification using single qubit encoding, *IEEE Transactions on Neural Networks and Learning Systems* 35 (2) (2024) 1472–1486. doi:10.1109/TNNLS.2022.3179354.

- [39] S. McFarthing, A. Pillay, I. Sinayskiy, F. Petruccione, Classical ensembles of single-qubit quantum variational circuits for classification, *Quantum Machine Intelligence* 6 (2) (2024) 81. doi:[10.1007/s42484-024-00211-x](https://doi.org/10.1007/s42484-024-00211-x).
- [40] M. P. Cuéllar, What we can do with one qubit in quantum machine learning: ten classical machine learning problems that can be solved with a single qubit, *Quantum Machine Intelligence* 6 (2) (2024) 76. doi:[10.1007/s42484-024-00210-y](https://doi.org/10.1007/s42484-024-00210-y).
- [41] E. Knill, R. Laflamme, Power of one bit of quantum information, *Phys. Rev. Lett.* 81 (1998) 5672–5675. doi:[10.1103/PhysRevLett.81.5672](https://doi.org/10.1103/PhysRevLett.81.5672).
- [42] M. A. Nielsen, I. L. Chuang, *Quantum computation and quantum information*, Cambridge University Press, New York, 2000.
- [43] N. H. Nguyen, E. C. Behrman, M. A. Moustafa, J. E. Steck, Benchmarking neural networks for quantum computations, *IEEE Transactions on Neural Networks and Learning Systems* 31 (7) (2020) 2522–2531. doi:[10.1109/TNNLS.2019.2933394](https://doi.org/10.1109/TNNLS.2019.2933394).
- [44] M. Redmond, A. Baveja, A data-driven software tool for enabling cooperative information sharing among police departments, *European Journal of Operational Research* 141 (3) (2002) 660–678. doi:[10.1016/S0377-2217\(01\)00264-8](https://doi.org/10.1016/S0377-2217(01)00264-8).
- [45] L. McClendon, N. Meghanathan, Using machine learning algorithms to analyze crime data, *Machine Learning and Applications: An International Journal* 2 (2015) 1–12. doi:[10.5121/mlaij.2015.2101](https://doi.org/10.5121/mlaij.2015.2101).
- [46] A. Kolomoitseva, [Statistical analysis of the communities and crime data set](#), Preprint from University of Alabama (April 2021).
URL https://www.researchgate.net/publication/354739856_Statistical_Analysis_of_the_Communities_and_Crime_Data_Set
- [47] R. Gonzalez, R. Woods, *Digital Image Processing*, Pearson, New York, NY, USA, 2018.